JGR Space Physics

RESEARCH ARTICLE
10.1029/2019JA027584

Solar Energetic Proton Access to the Near-Equatorial Inner Magnetosphere

Rachael J. Filwett[1], Allison N. Jaynes[1], Daniel N. Baker[2], Shrikanth G. Kanekal[3], Brian Kress[4], and J. Bern Blake[5]

[1]Department of Physics and Astronomy, University of Iowa, Iowa City, IA, USA, [2]Laboratory for Atmospheric and Space Physics, University of Colorado Boulder, Boulder, CO, USA, [3]NASA Goddard Space Flight Center, Greenbelt, MD, USA, [4]Cooperative Institute for Research in Environmental Science, Boulder, CO, USA, [5]The Aerospace Corporation, El Segundo, CA, USA

Key Points:
- Small flux substructures in interplanetary space are observed in the inner magnetosphere
- West-to-east flux ratios are used as a proxy for cutoff location and energy
- West-to-east flux ratios are highly dynamic from orbit to orbit and respond quickly to magnetospheric changes

Correspondence to:
R. J. Filwett,
rachael-filwett@uiowa.edu

Citation:
Filwett, R. J., Jaynes, A. N., Baker, D. N., Kanekal, S. G., Kress, B., & Blake, J. B. (2020). Solar energetic proton access to the near-equatorial inner magnetosphere. *Journal of Geophysical Research: Space Physics*, *125*, e2019JA027584. https://doi.org/10.1029/2019JA027584

Received 29 OCT 2019
Accepted 5 MAY 2020
Accepted article online 17 MAY 2020

Abstract In this study we examine the ability of protons of solar origin to access the near-equatorial inner magnetosphere. Here we examine four distinct solar proton events from 20–200 MeV, concurrent with both quiet time and storm time conditions using proton data from the ACE satellite in the solar wind upstream of Earth and data from the Relativistic Electron Proton Telescope (REPT) instrument aboard Van Allen Probes. We examine the direct flux correspondence between interplanetary space and the inner magnetosphere. Small substructures in interplanetary space are observable in the REPT flux profiles, which can penetrate down to L values of $\leq$4. Furthermore, there are orbit-to-orbit variations in the west-to-east anisotropic flux ratios. The anisotropic flux ratios are used as a proxy for cutoff energies and display cutoff variations with L shell and energy. The dependence of the anisotropic flux ratio on *Dst* values is shown. The results paint a picture of highly dynamic spatial and temporal proton cutoff rigidities in the near-equatorial inner magnetosphere.

1. Introduction

Solar proton events are initiated by energetic protons of solar or interplanetary (IP) origin which are able to access the magnetosphere. These solar energetic particles (SEPs) are released at the Sun during times of active periods in associating with a solar flare or coronal mass ejection (CME). It is generally accepted that there are two types of SEP events: impulsive and gradual with the former being accelerated by magnetic reconnection in flares and the latter by CME shocks (Reames, 1999). SEPs are a space weather hazard with risks to both manned and robotic space assets. SEPs can damage electronic equipment and expose astronauts and airline passengers to increased levels of radiation and may have global effects on the atmosphere (Reames, 1999; Shea & Smart, 2012). The ability of a proton to access the magnetosphere is dependent upon its incident rigidity, which is measured in momentum per charge. The cutoff rigidity is the threshold rigidity below which the particle fluxes are essentially 0 due to geomagnetic shielding. Each altitude, magnetic local time (MLT), L value, magnetic latitude, and particle arrival direction corresponds to a specific cutoff rigidity (Störmer, 1955).

Access of SEPs to low altitudes, particularly near the polar cap boundary, has been extensively discussed in the literature, but the access to the near-equatorial inner magnetosphere has had considerably less study. Early predictions, particularly by the Störmer theory, indicated that proton fluxes in the equatorial magnetosphere should have been much lower than data indicated by early satellite missions. Fillius (1968) found that an increased field associated with the symmetric ring current should hinder SEP access to the near-equatorial inner magnetosphere. The first measurements of solar proton fluxes at geosynchronous orbit indicated that solar protons penetrate much further into the magnetosphere than predicted by Störmer theory (Lanzerotti, 1968; Lanzerotti, 1972; Paulikas & Blake, 1969). Measurements made with detectors aboard the ATS-1 spacecraft indicated that protons with $E > 21$ MeV are not magnetically shielded at geosynchronous orbit, and for protons that are 5–21 MeV there is partial shielding, with a diurnal flux variation that approaches the IP SEP flux near midnight MLT (Paulikas & Blake, 1969).

In this study we look at four solar proton events, 6–9 January 2014, 21–23 June 2015, 6–9 September 2017, and 10–13 September 2017. These four events were selected because they represent some of the strongest solar proton events during the Van Allen Probes era. Additionally, these events are associated with a

variety of IP and geomagnetic conditions, such as *Dst*, maximum proton flux, structure of precipitating event, and maximum proton energy. Due to the strength of these four events, most have been discussed extensively in the literature; in particular, the 10–13 September 2017 event has been the subject of many studies (see Space Weather special issue "Space Weather Events of 4–10 September, 2017"). This event was classified as a GLE (ground level event) because the proton energy spectrum extended to high enough energies that ground-based neutron monitors measured the secondary particles. The proton spectra (Cohen & Mewaldt, 2018) and access into the near-equatorial magnetosphere with respect to particle energy, location, and direction of incidence (O'Brien et al., 2018) have been examined, along with an effort to model particle cutoff locations by matching Van Allen Probes data (Qin et al., 2019). This event was so pervasive that it was measured over a wide range of energies by near-Earth satellites and ground-based monitors, allowing for comprehensive cross comparison of in situ detector data (Jiggens et al., 2019).

In this study we examine the proton access into the magnetosphere by looking at the flux substructure in solar proton events by comparing the time-intensity profiles of Relativistic Electron Proton Telescope (REPT) and ACE/SIS. We also investigate the east-west anisotropy seen by eastward and westward facing particle telescopes, similar to the recent work of Qin et al. (2019). These anisotropies are used to examine the proton cutoffs as a function of MLT, L value, energy, and *Dst*. Here we examine a broad range of solar proton events in the near-equatorial inner magnetosphere to give a more complete picture of the conditions affecting energetic particle magnetospheric access.

1.1. Theoretical Consideration

Geomagnetic shielding of energetic ions incident upon Earth from outside the magnetosphere is quantified in terms of cutoff rigidity. Cutoff rigidity is the threshold below which the energetic particle flux (originating outside of the magnetosphere) is 0. Cutoff rigidity is a function of location, direction of particle arrival, and geomagnetic activity. In the simplistic case of a purely dipole field the cutoff rigidity can be expressed as

$$R_c = C_{st}\frac{1}{L^2}\frac{1}{\left(1+\sqrt{1+\cos\alpha\cos^3\lambda}\right)^2} \tag{1}$$

where L is the dipole L value, λ is the magnetic latitude, α is the angle between the particle arrival direction and magnetic west, and $C_{st} = 60$ is a constant containing the dipole moment and the conversion factors necessary to express R_c in units of GV (Störmer, 1955). Although rigidity is the fundamental unit that determines a charged particle path in a magnetic field, it is often more convenient to discuss cutoffs in terms of cutoff energy, E_c, which is how it will be discussed here. The Störmer theory is heavily dependent upon its description of the Earth's magnetosphere as a dipole in equilibrium, which, although a reasonable first-order approximation, is not completely accurate. The Earth's magnetic field is also highly responsive to changes in solar wind conditions, which is not accounted for in Equation 1.

Cutoff analysis in a magnetic field shows that the cutoff energies are lowest for the westward direction and are higher for the eastward field of view (FOV) (Kress et al., 2013). This is because MeV ions incident upon a detector from the east have lower gyrocenters and so must penetrate significantly further into the magnetosphere than ions arriving from the west. The resultant effect is an east-west asymmetry which manifests during SEP events as substantially different fluxes observed by east or west facing proton telescopes, with the exception of low Earth orbit (LEO) where there is little variation in SEP cutoffs with direction of arrival (Blake et al., 1974; Kress et al., 2013; Rodriguez, 2012; Rodriguez et al., 2010). Since 1998, the GOES observatory system has collected eastward and westward observations of MeV solar proton fluxes. The Energetic Particle Sensors (EPS) on GOES 8–12 have a single westward FOV (Sellers & Hanser, 1996; Onsager et al., 1996). Since January 1998, the GOES 10 EPS FOV was directed eastward allowing simultaneous eastward and westward observations. GOES 13 with its Energetic Proton, Electron and Alpha Detector (EPEAD) instrument has both an eastward looking and westward looking telescope giving the capability of simultaneous temporal-spatial measurements in the east and west directions. Using GOES 9, 10, 11, and 13 data, Rodriguez et al. (2010) found that the east-west flux ratio is sensitive to geomagnetic activity, approaching unity at geosynchronous equatorial orbit (GEO) during times of enhanced *AE* index activity. Rodriguez et al. (2010) also showed that the west flux could be an order of magnitude greater than the flux from the east. Furthermore, Rodriguez (2012) illustrated that variations in the east-west flux ratio were due to

substorm-related magnetic field changes in the near-Earth magnetotail that enhance access of SEPs to the inner magnetosphere. Additionally, Ogliore et al. (2001) reported on vertical cutoffs for rigidities from ~500 to 1,700 MV using SAMPEX data and found that cosmic rays can penetrate several degrees lower in latitude than estimated by most quantitative relations representing geomagnetic cutoff. Ogliore et al. (2001) empirically found that $R_c = 15.062\cos^4(\Lambda) - 0.363$ GV, where R_c is the magnetic cutoff rigidity and Λ is the invariant latitude. Qin et al. (2019) examined access of solar protons to the inner magnetosphere on 11 September 2017 using Van Allen Probes/REPT data and by computing reverse particle trajectories with the Dartmouth geomagnetic cutoff code (Kress et al., 2010). Qin et al. (2019) found that cutoff latitude is lower for solar protons with higher energy and that access to the inner magnetosphere is strongly dependent on particle arrive direction relative to magnetic west. Qin et al. (2019) examined the relationship between energy and L shell access and found that a small number of protons of the 11 September 2017 event are below the relationship found by Ogliore et al. (2001).

Direct particle entry along the open magnetic field lines is the basic mechanism which describes the entry of solar protons into the magnetosphere (Paulikas, 1974). Solar wind particles with large gyroradii can enter directly across magnetic field lines, which is the type of entry discussed by cutoff theory. Additionally, high-energy particles can also gain access to the magnetosphere across magnetic field lines by a slow diffusion-like process (Scholer, 1975). Results from particle tracking models (Richard et al., 2002) indicate that energetic particles (0.1 to 50 MeV) can directly penetrate the magnetosphere along open field lines, while more energetic particles ($E > 10$ MeV) can gain access to the dayside magnetopause due to large Larmor radii. Kalegaev et al. (2018) showed a comparison of the fluxes measured at geostationary and polar orbits, which indicated different access pathways for the particles detected at high and low latitudes. The observed energetic particle transmission to the low latitudes during solar proton events can be explained by both direct penetration on open field lines and diffusive-like transport of fluxes deep into the inner magnetosphere, although the relative contribution of each entry method is not yet well understood. Kress et al. (2005) presented a mechanism of prompt trapping of SEPs during storm time periods. During these periods, SEPs can be impulsively injected into low L values by sudden compression of the magnetosphere. The results indicate that solar wind P_{dyn} plays a significant role in the observed injection of ions to low L values (Hudson et al., 2004). SEP entry has a great variety of observed dynamical behavior, with asymmetries of particle flux amplitudes while entering the magnetosphere (Pereyaslova, 1982). Increased ring current (represented by *Dst*), auroral activity (as indicated by the *AE* index), and P_{dyn} have all been correlated with suppressed cutoffs (Kress et al., 2004, 2010; Leske et al., 2001). These suppressed cutoffs have also been associated with solar proton fluxes approaching west-east isotropy at geosynchronous orbit (Kress et al., 2013; Rodriguez, 2012; Rodriguez et al., 2014, 2010).

2. Methodology

The four events studied here occurred on 6–9 January 2014, 21–23 June 2015, 6–9 September 2017, and 10–13 September 2017. This study uses solar proton data from the REPT (Baker et al., 2013) from the Energetic Particle, Composition, and Thermal Plasma Suite (ECT) (Spence et al., 2013) on Van Allen Probes. The Van Allen Probes were launched in August 2012 into an ~600 × 33,000 km orbit with an inclination of 10.2°. This study utilizes data from both of the identically instrumented Van Allen Probes satellites, labeled "A" and "B." The full energy range of the REPT instrument is utilized with eight proton energy channels having a range from 18.5 MeV in the lowest energy channel up to >116 MeV in the highest integral energy channel. The primary REPT science data provide particle counts for each energy bin, for each spin, which is subdivided into 36 sectors of equal duration. Along with the spin-averaged and spin-resolved REPT proton data products, we use the relative position of the REPT telescope on the spacecraft to transform the coordinates for the spin-resolved data to a flux given in pointing direction in Geocentric Solar Ecliptic (GSE) coordinates. This transformation is used to identify particles that are coming from the east (west) which are arriving from the duskward (dawnward) side of the magnetosphere putting their gyrocenter closer (further) from Earth than the satellite's instantaneous location. We note that the spin axis of RBSP is generally pointed along the Sun-Earth line but can vary up to 10.5°, with a rate of change of approximately 1° per day. The spin plane throughout the full orbit samples particles in the *y-z* plane in GSE, and there is an inherent error using particles arrival direction from GSE due to the discrepancy of the magnetic equator compared to the equatorial plane. Since we are using a 90° acceptance range, 45° above and below axis, the analysis method used here is

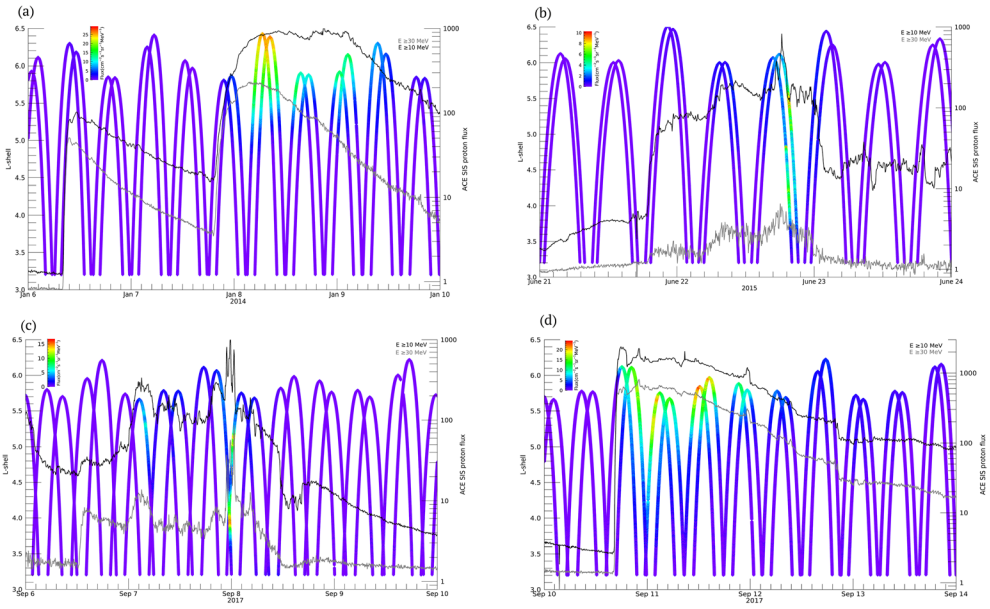

Figure 1. The 21.25 MeV spin-averaged proton flux mapped onto their associated L values for the four solar protons events focused on in this study: (a) 6–9 January 2014, (b) 21–23 June 2015, (c) 6–9 September 2017, and (d) 10–13 September 2017. The ACE/SIS $E \geq 10$ MeV (black) and $E \geq 30$ MeV (gray) proton flux are shown.

still capturing the proton flux coming from magnetic east (west). Any directional pointing discrepancies are captured by both the eastward and westward flux acceptance ranges, so the east/west ratio used here as a proxy for cutoffs should be minimally affected. When RBSP is off of the noon-MLT line the east (west) GSE particle measurements still represent gyrocenters inside and outside of the spacecraft L shell, but there is a MLT difference in the particle gyrocenters. This is a particular issue for the June 2015 event, but for the other events the REPT measurement spin plane is approximately east/west. The offset of the measurement angle relative to east (west) changes constantly during orbit, particularly as the spacecraft adjusts to keep the spin axis within 10.5° of Sun pointing. There is some contamination in the low-energy proton channels due to penetration of high-energy particles from outside the instrument FOV; this is an issue particularly near the inner proton belt. This region can also be the lower boundary of an individual solar proton event. Improper handling of this known source of error could lead to misinterpretation of cutoffs at low L values; for the stated reasons we do not use this flux as an exact map of the cutoffs but rather as a proxy to understand dynamical changes.

Here we also utilize ACE/SIS observations to give a representation of the IP energetic proton conditions upstream of Earth. The SIS data product is two integrated proton energy channels at $E \geq 10$ and $E \geq 30$ MeV; the SIS measurements do not include angular distributions for energetic particles, but in absence of a superior data product this suffices. Including data from multiple spacecraft allows comparison of proton time-intensity profiles. For solar proton events, when we are considering how particles may access the inner magnetosphere, it is vital to have a baseline understanding of the particle conditions in near-IP space.

3. Results

Figure 1 shows the 18.4–24 MeV flux observed by REPT-A and REPT-B as a function of the spacecrafts McIlwaine's L shell parameter, calculated using the International Geomagnetic Reference Field (IGRF) model based on TS05. The events seen in Figure 1 occurred on 6–9 January 2014 (a), 21–23 June 2015 (b), and 6–13 September 2017 (two events; c and d). The two September events originate from the same active region on the Sun but are separated in time by multiple days and have very different characteristics making it appropriate to analyze them independently. Two events (Figures 1b and 1c) are very impulsive in nature with rapid flux changes, and two events appear more typical of an SEP event impinging on the magnetosphere (Figures 1a and 1d). Large events are often observed with a strong shock front which rapidly

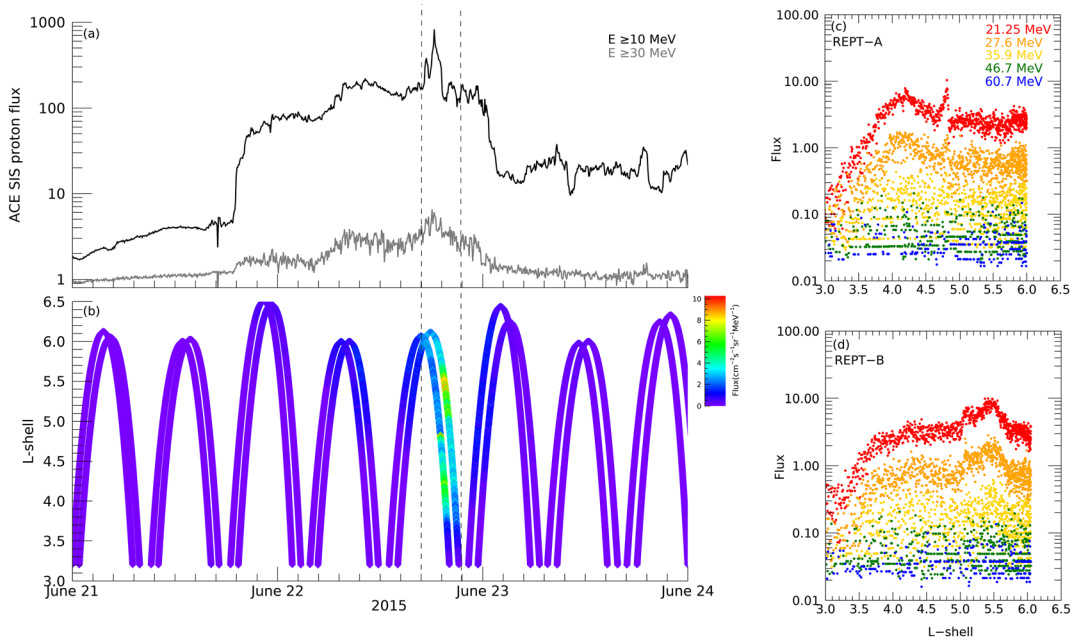

Figure 2. The 21.25 MeV REPT proton flux (b) and ACE/SIS $E \geq 10$ MeV (black) and $E \geq 30$ MeV (gray) (a) for the event occurring on 21–23 June 2015. Two selected half orbits, the timing of which is indicated by dotted lines in (a) and (b), for the inbound passes of REPT-A and REPT-B at five energy channels (21.25–60.7 MeV) are shown in panels (c) and (d) at the left. In the single orbital plots we see the spatial and energy dependence of the IP flux direct correspondence substructures.

comes to a maximum in energetic particle intensity and then has a gradual decrease in intensity over a matter of hours or days. The two impulsive events, 21–23 June 2015 and 6–9 September 2017, in Figures 1b and 1c, have a more complex substructure with some midevent acceleration, which is most likely the result of a solar flare-like event. Here we do not use the words "gradual" or "impulsive" to classify the precipitating solar source but rather to describe the rate of the changing proton flux in the magnetosphere. Two of the four events in this study are associated with geomagnetic storms, 21–23 June 2015 ($Dst \sim -200$) and 6–9 September 2017 ($Dst \sim -150$), while the other two are associated with much quieter geomagnetic conditions.

3.1. Direct Flux Correspondence

Liouville's theorem requires that the flux of particles at rigidities above the cutoff rigidity is the same as in IP space (Lemaitre & Vallarta, 1933; Swann, 1933). When $E < E_c$, the flux should be 0, and when $E > E_c$, the flux should be the same as IP space, where E_c is a directionally dependent proton cutoff energy. This implies that any small change in IP flux should be mirrored in the observed magnetospheric fluxes. The resultant observable would be small changes in flux, or energy spectrum, and should be seen in the magnetosphere as a direct flux correspondence. The ACE spacecraft which is located upstream of Earth at $L1$ gives a good representation of what is upstream from Earth, but it does not necessarily represent the exact conditions that will be incident upon the magnetosphere; additionally, this study cannot account for angular distributions of protons at $L1$. Figure 1 shows the flux inside the magnetosphere quickly responding to the changing IP flux observed at ACE. The substructure or changes in the spatiotemporal proton time-intensity profile at ACE and then observed by REPT are seen in Figure 1 on inbound/outbound orbits penetrating deep into the near-equatorial magnetosphere. The two strong impulses on 22 June 2015 (Figure 1b) are mimicked on the inbound leg of the Van Allen Probes orbit. The three distinct impulses on 7–8 September 2017 (Figure 1c) are seen as proton flux increases permeating down to $L < 4$. In these impulsive SEP-type events it is unsurprising that the same flare-like substructure would show up in the magnetospheric proton flux.

Figure 2a shows the flux as a function of L value in time with the co-timed ACE/SIS data. Figures 2b and 2c show the flux versus L value at 21.25–60.7 MeV for both Van Allen Probes A and B on 22 June 2015. Figures 2b and 2c each show one inbound orbit for REPT-A and REPT-B, displaying the energy extent of

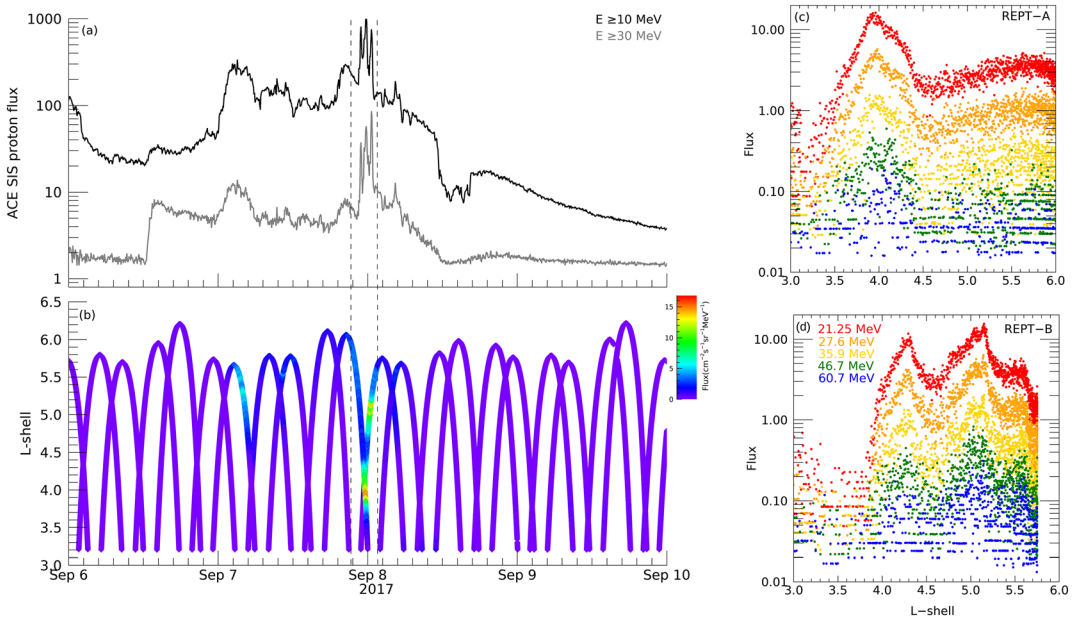

Figure 3. The 21.25 MeV REPT proton flux and ACE/SIS $E \geq 10$ MeV (black) and $E \geq 30$ MeV (gray) for the event occurring on 6–9 September 2017. Two selected half orbits for an inbound pass of REPT-A and an outbound pass of REPT-B, the timing of which is indicated by dotted lines in (a) and (b), at five energy channels (21.25–60.7 MeV) are shown in panels (c) and (d) at the right. In these single orbital plots, we see the spatial and energy dependence of the IP flux direct correspondence substructures.

these substructures. The impulsive nature of the IP flux results in a spike in fluxes in the REPT data, to the point of becoming a near discontinuity. In the selected orbits there are small, but perceptible, proton flux changes that can be mapped back onto the IP space proton flux. The correspondence of the temporal development of particle fluxes observed by ACE and by GOES, and to some extent POES-17, was also noted looking at the January 2005 SEP event (Kalegaev et al., 2018). In the June event shown in Figure 2 there are two strong flux peaks seen in Figure 2c, strongly associated with the double peak flare structure in the ACE data in panel Figure 2a. These flux peaks gain access to $L = 4$. This is particularly true of the two impulsive events in this study, which are also associated with geomagnetic storm conditions.

Figure 3 is the same format as Figure 2 but shows substructure for minor flux changes during the 6–9 September 2017 event. Figure 3a shows the inbound orbit L profile for 21.25 MeV for REPT-A and REPT-B and the co-timed IP energetic proton flux. Figures 3c and 3d show a half orbit profile of flux versus L value for REPT-A and REPT-B for 21.25–60.7 MeV protons. In Figure 3d the REPT-B outbound orbit has three low-intensity but distinct flux peaks associated with sudden peaks in the IP protons. The peaks in Figure 3d can be seen in multiple energies with clear solar proton structure at $L \sim 4.2$ and above, but REPT-A observes a single peak at $L < 4$. The orbital timing with inbound versus outbound configuration influences the observation of these proton impulses. When examining the REPT-B L value versus flux plot in Figure 3d, we can see two distinct peaks at ~4.2 and 5.1 L in the lower energies along with sharp flux drop near apoapsis, but when we examine the higher energies (46.7+ MeV), there are three distinct peaks. The relative height of the peaks changes with energy, which corresponds to the ACE data because the third dramatic proton flux is more intense at $E \geq 30$ MeV than it is for the previous rapid flux increases. This implies that we are seeing not only the substructures in the IP data but also the spectral changes directly in the REPT proton data. This direct flux correspondence can be seen during the 6–9 September 2017 event, prior to the onset of a geomagnetic storm. This implies that this direct flux correspondence is not driven by *Dst* changes in the cutoff rigidities but rather is driven by variation in the IP SEP flux.

In Figure 4 during the 10–13 September 2017 event there are small substructures in the IP protons which are then observed by REPT. The changes in the proton flux at ACE are so small it is difficult to say with certainty that this is the precipitating cause of the flux structure seen in Figure 4c. When we examine this and other

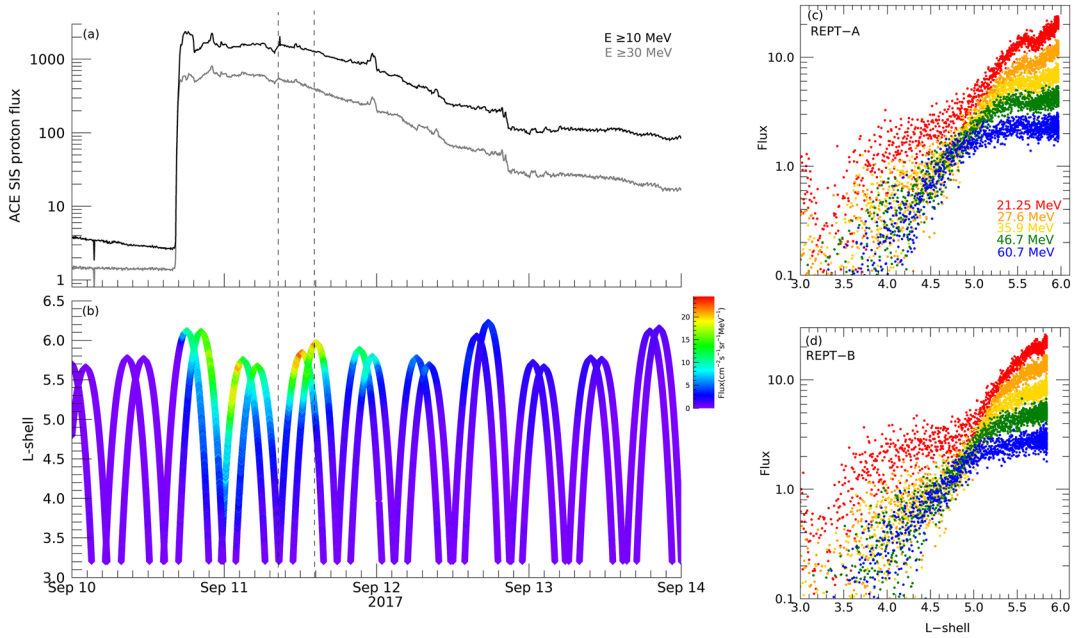

Figure 4. The 21.25 MeV REPT proton flux and ACE/SIS $E \geq 10$ MeV (black) and $E \geq 30$ MeV (gray) for the event occurring on 10–13 September 2017. Two half orbits, the timing of which is indicated by dotted lines in (a) and (b), for the outbound passes of REPT-A and REPT-B at five energy channels (21.25–60.7 MeV) are shown in panels (d) and (c), respectively. In these single orbital plots, we see the spatial and energy dependence of the IP flux direct correspondence substructures.

orbits for this event, it is clear that the substructure is quite similar to these microchanges at ACE, demonstrating the sensitivity of the innermagnetosphere to changes in proton flux. These flux substructures are extremely transient and are related with small proton substructure at ACE but certainly do not exhibit a fully one-to-one correlation as predicted by Liouville's theorem, assuming we are measuring above the cutoff energy. The correlation between ACE/SIS proton flux and REPT flux may be obfuscated by orbital positions and spacecraft phasing and any inherent flux differences between what is observed at $L1$ and what is impinging upon Earth. Furthermore, it can be seen in Figures 2–4 that the substructures are not fully resolved at the lowest L values. When we compare panels (c) and (d) in Figures 2–4, we see that in Figures 4c and 4d the flux drops off more rapidly in the inner magnetosphere. This is attributed to the quiet time conditions during this storm, whereas there is a geomagnetic storm concurrent with Figures 2 and 3, allowing for significant particle entry into the inner equatorial magnetosphere. Even considering the quiet time conditions, it is puzzling why some substructures are visible while others, which seem like they should be visible, are not. The visibility of substructures could be related to minor changes in magnetospheric conditions such as the tail configuration as found in Rodriguez (2012), differences between the IP conditions at ACE and Earth, or the method of entry into the inner equatorial magnetosphere. Further studies would be needed to fully characterize why energetic particle substructures are not always visible and would require examining a wide range of solar wind and magnetospheric plasma conditions, along with using data multiple spacecraft to understand temporal structures.

3.2. Implied Cutoffs Using East-West Anisotropies

Figure 5 shows the spin sector resolved flux for the solar proton event of 6–9 January 2014 integrated over the full REPT energy range of 20–200 MeV. Here we examine $L \geq 3.2$ as to limit contamination from the penetrating high-energy protons near the inner radiation belt. In Figure 5 we define particles arriving from magnetic west (east) to be within a 90° (±45°) of the direction perpendicular to the satellite position vector and the vertical axis in GSE coordinates (further details on the point direction flux data product can be found in section 2). In Figure 5 it is apparent that protons arriving from the westward direction have a higher flux than those arriving from eastward direction. This is because protons arriving from the west have

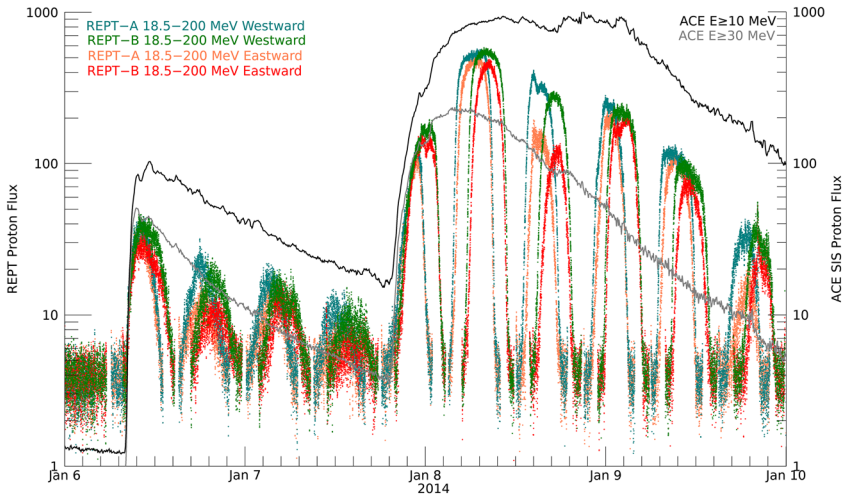

Figure 5. The energy-integrated directional flux for the westward and eastward directions for both REPT-A and REPT-B. The westward and eastward fluxes are defined as being within a 90° FOV centered at due west and due east. The flux for the eastward direction associated with REPT-A is orange, and REPT-B is red, with the westward directional flux for REPT-A in blue, and REPT-B is shown green. The ACE/SIS $E \geq 10$ MeV (black) and $E \geq 30$ MeV (gray) fluxes are also shown. The L value range show here is >3.2.

gyrocenters above the spacecraft, whereas those arriving from the east have gyrocenters below the spacecraft where their flux is reduced due to additional geomagnetic shielding. In Figure 5 the relative flux between eastward and westward arriving particles varies greatly over time.

Figure 6 shows the west/east anisotropic flux ratios associated with $L > 3.2$ along with the ACE/SIS $E \geq 10$ MeV proton flux. The west and east fluxes have had a smoothing function applied, with a character time of 77 s, prior to taking the directional ratio. This smoothing function highlights the general trends of the west/east flux ratio which occur on the scale of tens of minutes to hours, while minimizing the appearance of outliers. At the peak of solar proton activity, the anisotropic ratio time profile takes on a characteristic "M" shape. If the satellites are measuring particles above the cutoff energy, with respect to both MLT and

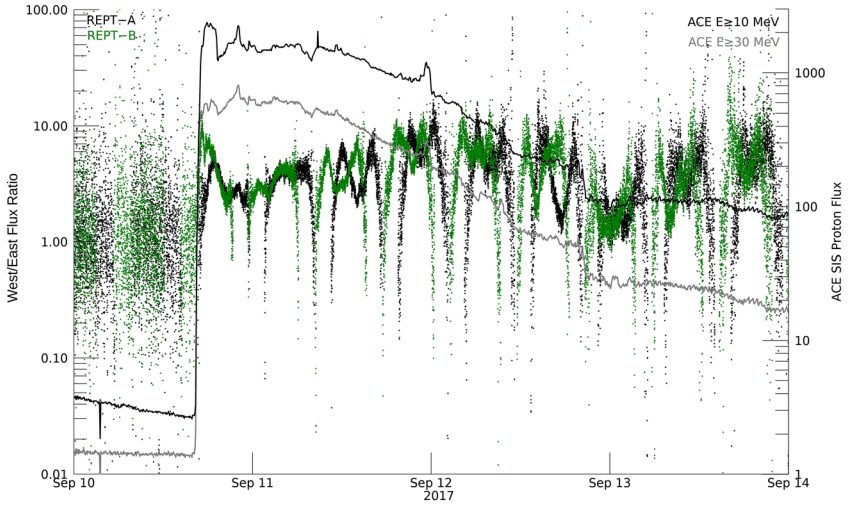

Figure 6. The ratio of west-to-east flux, integrated over the full REPT energy range of 20–200 MeV for 10–13 September 2017. The black dots represent the flux ratio for REPT-A and green dots representing the ratio for REPT-B. A smoothing function was applied to both the east and west fluxes before the ratio was taken. The data here represent $L > 3.2$. The ACE/SIS flux at $E \geq 10$ MeV (black) and $E \geq 30$ MeV (gray) is also shown with its accompanying y axis on the right.

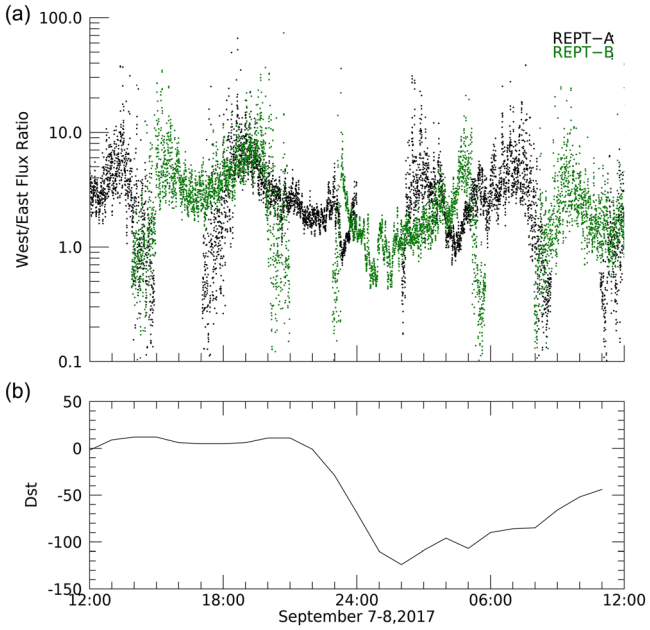

Figure 7. The ratio of west/east flux integrated over the entire REPT energy range for 1 day during the solar proton event of 7–8 September 2017 is shown in the top panel. The *Dst* on the same day is shown in the bottom panel. There is a less pronounced "M" shape, with sudden decreases in the flux ratio most likely corresponding to magnetic topological changes associated with geomagnetic storm onset. There are complex anisotropic flux ratio changes after 23:00 particularly for REPT-B.

altitude, the expectation would be a ratio of 1 (isotropy). At times of no solar proton activity the ratio is highly dynamic as seen on 10 September prior to event onset, which could at least partially be contributed to the low statistics in the overall particle count rate. The "M" shape is created as the satellite moves from low *L* values; they start to see protons arriving from the westward direction. The ratio is at a maximum when the satellite is at an altitude where it is measuring westward particles, but few particles from the east have made it past the cutoff. The ratio then decreases at high *L* values as both particles from the eastward and westward directions can be observed by the REPT telescopes. Figure 6 indicates that at apogee, the cutoff is above the lower-energy bound of the REPT proton measurements. We note that at the lowest *L*, for low proton energies, the ratios are subject to contamination, but we are looking at the full instrument range of proton energies and are interested in the overall trend of the west/east ratios. At very low *L*, and prior to event onset the flux ratio appears to be significantly below 1, this is attributed to low flux count noise. Qin et al. (2019) also examined the east-west dependence for this event, utilizing REPT data and particle tracking simulations. Qin et al. (2019) found that solar protons at higher energies have less east-west dependence at the apogee of the satellites compared to lower-energy protons, indicating that the higher-energy protons experience less shielding by the magnetic field and are above the cutoff. Similarly, here the west/east flux ratio, which appears as a characteristic "M" shape, illustrates that the cutoff rigidity depends strongly upon particle direction of arrival and *L* value (Kress et al., 2013; Rodriguez et al., 2010).

Figure 7 shows the west/east ratio and the hourly *Dst* values for a 24 hr period of the 6–9 September event. The same smoothing function and data limits were used in Figure 7 as in Figure 6. In both 21–23 June 2015 and 6–9 September 2017 there are strong geomagnetic storms that occur simultaneously with solar proton access. The 6–9 September 2017 event shows how the west/east flux ratio, a proxy for particle cutoff energy, responds to the rapidly changing storm conditions. It is clearly seen at the incoming portion of REPT-A's orbit that the characteristic "M" shape of the west/east ratio fails to produce a well-defined second peak due to a sudden flux ratio decrease. The flux ratio for REPT-B becomes more sporadic slightly after midnight as the *Dst* continues to drop. These changes indicate a topological change in the magnetic field that is quickly modifying cutoff locations, bringing the anisotropic ratio closer to unity. This same change in cutoff location occurs during the 21–23 June 2015 event. The two events that have large changes in *Dst* are also impulsive events due to the rapidly changing IP particle conditions. In the future a larger statistical study of more solar proton events observed with Van Allen Probes may be able to decouple the magnetic topological changes with *Dst* versus the particle forcing of highly impulsive events.

Figure 8 shows the west/east flux ratio mapped onto the *L* value for all of the events examined in this study occurring 6–9 January 2014, 21–24 June 2015, 6–9 September 2017, and 10–14 September 2017 and the simultaneous *Dst* values. In the January event the structure of the west/east ratio, for 20–200 MeV, is observed to be at a maximum between 4.5 and 5 *L*. In Figure 8a during the inbound leg of the orbits there is a remarkably lower anisotropic flux ratio. This is most likely due to the location Van Allen Probes is orbiting in. During this event, the apoapsis of Van Allen Probes is in the afternoon sector of the magnetosphere, with the inbound leg on the duskside of the Earth, with the possibility of partial ring current affecting the west/east ratio. The other three events do not show similar orbit asymmetries of the cutoffs. The impulsive events of June (b) and 6–9 September 2017 (e) respond quickly to the changing *Dst* which is the driving factor in the location of the east-west asymmetries, as indicated by the current drops in *Dst* seen in (d) and (g). The 10–14 September 2017 event and the 10–14 January 2014 event last over several days and do not have any significant *Dst* changes. The notable difference between the events is that on 10–14 September 2017 the Van Allen Probes have their apoapsis at approximately noon MLT, while the January 2014 event has its

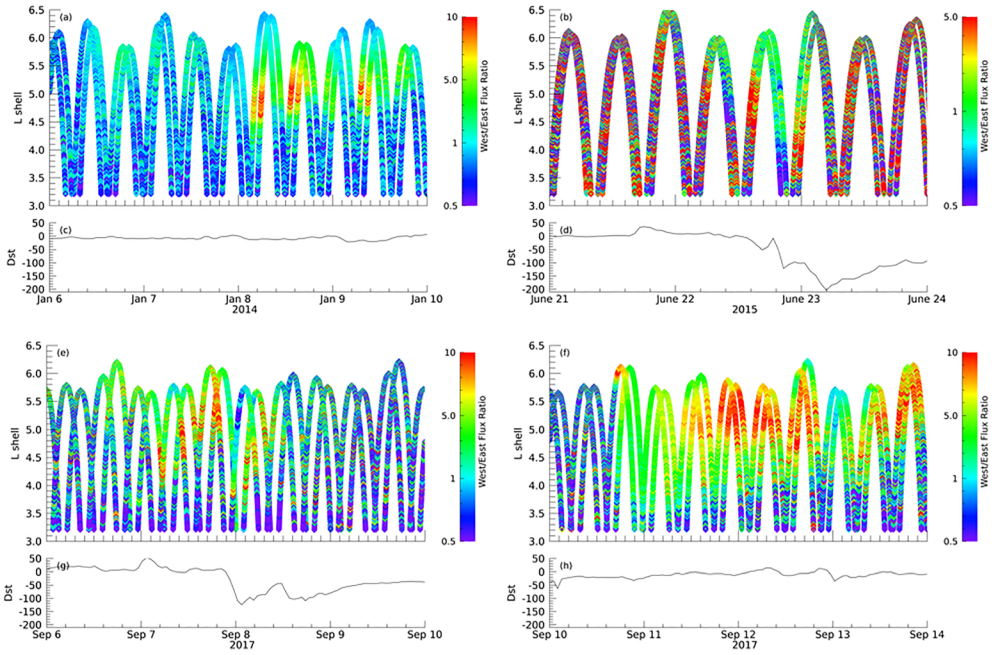

Figure 8. The west/east flux ratio for 20–200 MeV mapped out by *L* value. Panels (a) and (c) show the west/east ratio and simultaneous *Dst* values for 6–10 January 2014. Panels (b) and (d) show the west/east ratio and simultaneous *Dst* values for 21–24 June 2015. Panels (e) and (g) show the west/east ratio and simultaneous *Dst* values for 6–10 September 2017. Panels (f) and (h) show the west/east flux ratio and simultaneous *Dst* values for 10–14 September 2017. A smoothing function was applied to both the east and west fluxes before the flux ratio was taken for all events.

apoapsis between 14:00 and 15:00 MLT. We speculate that this orbital configuration, and hence the difference in MLT, is responsible for the cutoff orbital asymmetries during the 6–10 January 2014 event. During this event, the apoapsis of Van Allen Probes is in the afternoon sector of the magnetosphere, with the inbound leg on the duskside of the Earth, with the possibility of partial ring current affecting the west/east ratio. It is important to note that due to the measurement spin plane of REPT, when off the noon-MLT line, the west/east flux ratio still represents a magnetic shielding effect, but there is an MLT and gyrophase difference of the westward and eastward particles, which could be contributing to the observed effect. Finally, we note that in Figure 8f on the start of 13 September 2017 there does appear to be some difference in cutoff location compared to the previous orbits, which is most likely driven by the minor *Dst* shift (Δ *Dst* of 47) that occurred during at that time.

The west/east flux ratio dependence on *L* value is shown for 6–9 September 2017 in Figure 8e. Here, as *also shown* in Figure 7, we can see a drop in the anisotropic ratios that is associated with the onset of a geomagnetic storm (drop in *Dst*). At the onset of the event the maximum anisotropic ratio peak occurs between 4.0 and 4.5 *L* increasing to >5.5. This event has a more disorganized flux ratio structure, possibly due to the highly varied flux compared to the 6–9 January 2014 event seen in Figure 8a. There is also an asymmetric anisotropic flux in each orbit seen in this event, similar to Figure 8a. However, this asymmetry is not systemic to either the inbound or outbound pass, and unlike the event in January 2014, the apoapsis of Van Allen Probes is near noon in MLT. We conclude that this is most likely associated with the magnetospheric compression during this time rather than a systematic cutoff variation, as indicated by the *Dst* shown during this event in Figure 8c. These two very different proton events illustrate a number of things. First, that before/after the solar proton event, we are not seeing the anisotropic flux peak, implying that it is SEP particles subjected to magnetospheric cutoffs we are measuring and not some other internal magnetospheric structure. Second, with or without a geomagnetic storm, the *L* value associated with maximum anisotropic flux can change by 1 *L* or greater within a few orbits (~1 day). Finally, cutoff rigidity, as also demonstrated in Figure 7, can vary with *Dst* and possibly MLT.

Figure 9 shows the west/east flux ratio projected onto *L* value at multiple energies for a single day during the 10–13 September 2017 event. Figure 9 shows the anisotropic flux ratio behavior with respect to energy,

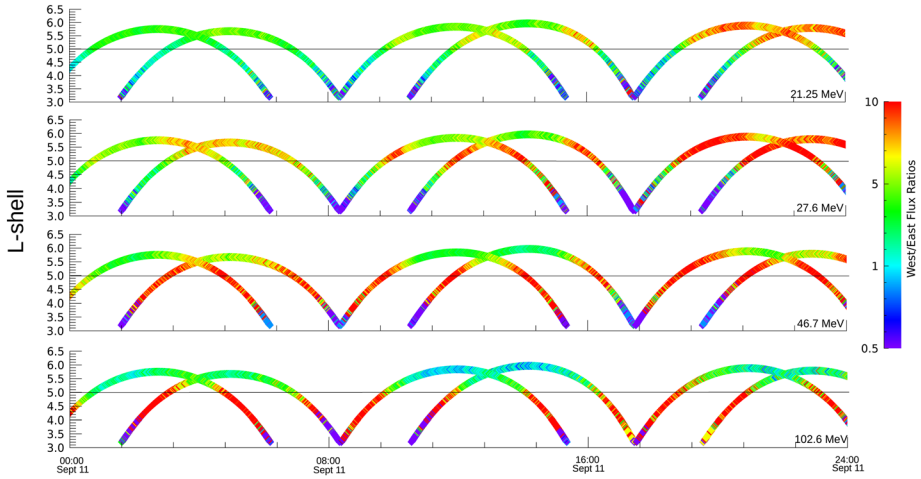

Figure 9. The ratio of west/east directional flux as a function of time and L value at 21.25, 27.6, 46.7, and 102.6 MeV during a portion of the solar proton event occurring on 11 September 2017. A line has been drawn at $L = 5$ at all four energies to serve as a visual guide.

whereas in Figures 6 and 7, the west/east ratio is integrated over the full REPT energy range. Figure 9 demonstrates that for the orbits shown, there is an energy dependence on the L value associated with maximum west/east flux ratios. The implication is that as proton energies increase, they are able to access lower L values and so the anisotropic ratio approaches unity at progressively lower altitudes. At 21.25 MeV the maximum flux ratios occur at $L > 5$, decreasing with energy until the maximum west/east flux ratio at 102.6 MeV is ~4.5 L. The west/east flux ratio is smaller near apoapsis at 102.6 MeV than the three lower energies shown in Figure 9. As previously mentioned, the 20–200 MeV anisotropic flux ratios shown in Figure 6 do not quite reach isotropy. As seen in Figure 9 this is not necessarily the case for higher energies, for the event shown, as they nearly reach isotropy. For this same event O'Brien et al., 2018 use data from the Relativistic Proton Spectrometer (RPS) (Mazur et al., 2013) on Van Allen Probes and found that higher-energy particles reach deeper into the magnetic field (have lower cutoff L). As a result, the gradient in the immediate vicinity to the spacecraft is smaller, which means there is less east-west asymmetry at $L > 5.5$ for high energies.

4. Discussion

4.1. Direct Solar Wind Correspondence

It is understood that if particles are able to gain access into the magnetosphere, in accordance with their cut-off energy, their flux should be equal to that of IP space. This is complicated by the inherent complexity in the cutoffs, as they can vary with *Dst*, MLT, *AE* index, P_{dyn}, particle energy, L value, and so forth. The direct correspondence observed between the full energy and intensity spectrum observed by ACE as compared to REPT is an expected observation. The observations show (e.g., in Figure 3) that a model of magnetospheric SEP flux based solely on cutoffs in a static geomagnetic field breaks down below $L \sim 4$ due to additional needed physics, for example, rapid inward radial diffusion or finite propagation time to low L in combination with rapid IP flux variations (as discussed in Morfill & Quenby, 1971).

We have considered the contamination in the proton channels that arise from permeating high-energy particles that originate from outside the FOV near the inner proton boundary; this error is negligible with our inclusion of data only above $L = 3$. Furthermore, during SEPs, high-energy protons can be registered in lower-energy channels, which we partially account for by examining only the integrated energy channels for the west/east flux ratio values. Additionally, the spin sector resolved data may be overcorrected for instrument dead time. When these sources of error are combined, the cutoff locations, particularly at low energies, may appear artificially closer to Earth. Due to this source of error, we do not put precise L values to the cutoff at each energy but rather examine the general trends and discuss ranges of cutoff values. Nonetheless, we would expect cutoff locations for these solar protons to be inherently diffuse rather than

sharp or discontinuous (Smart & Shea, 2005). Furthermore, the permeating high-energy particle error is mostly negated by this study's limitation in only considering $L > 3$. In the future using the PHA data analysis tools developed and utilized by Selesnick et al., 2014, Selesnick et al., 2018, and Qin et al., 2019, it might be possible to map cutoff locations over the REPT energy range with greater precision.

An important discussion that was not within the scope of this work was the potential effects radial transport might have on the appearance of these events. It is challenging to put limits onto the effects of radial transport due the highly transient nature of these events, specifically flux substructures. We know from previous work that protons reaching to $L \leq 4$ may emerge as a new inner proton belt at approximately $L = 3.5$, which is suggestive of a diffusive transport mechanism, such as drift-resonant radial transport. These new belts are short lived because they are easily removed by ring current perturbations (Hudson et al., 2004). This radial diffusion may be partially responsible for the diffusive nature of the observed substructures as they reach increasingly lower L values. Further discussion of the trapping of solar protons in the equatorial regions of outer edge of the inner proton belt is beyond the scope of this work.

4.2. Cutoff Energy

The majority of previous studies have focused on the geomagnetic cutoff latitude at LEO (Kress et al., 2010; Leske et al., 2001); this is in part due to the limited measurements in the equatorial plane prior to Van Allen Probes. In this study we examined the solar proton access to the near-equatorial inner magnetosphere. In a simplistic way we can think of particle entry into this part of the magnetosphere through three mechanisms: directly through open field lines at the cusps, across field lines due to large gyro radii in a static magnetic field (cutoff theory), and through a diffusive process at the dayside magnetopause for particles $E > 10$ MeV in a time-dependent magnetic field. These mechanisms may exist simultaneously and be more dominant during different phases of SEP onset or during various IP conditions (Kalegaev et al., 2018). All processes are extremely fast and could lead to similar west-east anisotropies.

In this study we have demonstrated the direct flux correspondence between IP flux and the flux observed in the near-equatorial inner magnetosphere. This direct flux correspondence is most evident at higher L values and applies to the full spectral range of energetic solar protons. We have shown observations that map the cutoff energies in the inner magnetosphere during quiet times and storm times and have shown an apparent asymmetry with MLT. During solar proton events, we have shown evidence that the cutoff rigidities may change rapidly due to changes in *Dst*. Furthermore, we have observationally demonstrated the energy dependence of the effectiveness of geomagnetic shielding at low L values. This finding is consistent with the work of Qin et al. (2019) which also found that the cutoff latitude is lower for solar protons with higher energy. These events are a small snapshot of the complete collection of the solar proton events observed with Van Allen Probes. The many parameters discussed that observationally affect cutoff rigidity locations would benefit from a larger statistical study that would also look at the *AE* index and P_{dyn} which have been documented to affect geomagnetic cutoffs. A subset of events, or a conglomeration of statistical findings, would also be benefited by a comprehensive modeling effort to capture the variability of these solar proton events.

Data Availability Statement

The data used here can be accessed at the Van Allen Probes Science Gateway (http://rbspgway.jhuapl.edu/) and the ACE data at CDAWeb (https://cdaweb.gsfc.nasa.gov/index.html/).

Acknowledgments

We would like to thank the reviewers for their thoughtful comments, which have improved the quality of this work significantly. This work was supported by the RBSP-ECT instrument under NASA Contract NAS5-01072. We would like to acknowledge the hard work and dedication of the Van Allen Probes and ACE teams in providing this comprehensive data source.

References

Baker, D. N., Kanekal, S. G., Hoxie, V. C., Batiste, S., Bolton, M., Li, X., et al. (2013). The Relativistic Electron-Proton Telescope (REPT) instrument on board the Radiation Belt Storm Probes (RBSP) Spacecraft: Characterization of Earth's radiation belt high-energy particle populations. *Space Science Reviews*, *179*(1-4), 337–381. https://doi.org/10.1007/s11214-012-9950-9

Blake, J. B., Martina, E. F., & Paulikas, G. A. (1974). On the access of solar protons to the synchronous altitude region. *Journal of Geophysical Research*, *79*(10), 1345–1348. https://doi.org/10.1029/JA079i010p01345

Cohen, C. M. S., & Mewaldt, R. A. (2018). The ground-level enhancement events of September 2017 and other large solar energetic particle events of cycle 24. *Space Weather*, *16*(10), 1616–1623. https://doi.org/10.1029/2018SW0020006

Fillius, R. W. (1968). Penetration of solar protons to four Earth radii in the equatorial plane. *Annales de Geophysique*, *24*, 821–840.

Hudson, M., Kress, B., Mazur, J., Perry, K., & Slocum, P. (2004). 3D modeling of shock-induced trapping of solar energetic particles in the Earth's magnetosphere. *Journal of Atmospheric and Solar-Terrestrial Physics*, *66*(15-16), 1389–1397. https://doi.org/10.1016/j.jastp.2004.03.024

Jiggens, P., Clavie, C., Evans, H., O'Brien, T. P., Witasse, O., Mishev, A. L., et al. (2019). In situ data and effect correlation during September 2017 solar particle event. *Space Weather*, *17*(1), 99–117. https://doi.org/10.1029/2018SW001936

Kalegaev, V. V., Vlasova, N. A., Nazarkov, I. S., & Melkova, S. A. (2018). Magnetospheric access for solar protons during the January 2005 SEP event. *Journal of Space Weather Space Climate*, *8*, A55. https://doi.org/10.1051/swsc/2018040

Kress, B., Hudson, M., Perry, K., & Slocum, P. (2004). Dynamic modeling of geomagnetic cutoff for the 23–24 November 2001 solar energetic particle event. *Geophysical Research Letters*, *31*, L04808. https://doi.org/10.1029/2003GL018599

Kress, B., Mertens, C., & Wiltberger, M. (2010). Solar energetic particle cutoff variations during the 29–31 October 2003 geomagnetic storm. *Space Weather*, *8*, S05001. https://doi.org/10.1029/2009SW000488

Kress, B., Rodriguez, J., Mazur, J., & Engel, M. (2013). Modeling solar proton access to geostationary spacecraft with geomagnetic cutoffs. *Advances in Space Research*, *52*(11), 1939–1948. https://doi.org/10.1016/j.asr.2013.08.019

Kress, B. T., Hudson, M. K., & Slocum, P. L. (2005). Impulsive solar energetic ion trapping in the magnetosphere during geomagnetic storms. *Geophysical Research Letters*, *32*, L06108. https://doi.org/10.1029/2005GL022373

Lanzerotti, L. J. (1968). Penetration of solar protons and alphas to the geomagnetic equator. *Physical Review Letters*, *21*(13), 929–933. https://doi.org/10.1103/PhysRevLett.21.929

Lanzerotti, L. J. (1972). Solar energetic particles and the configuration of the magnetosphere. *Reviews of Geophysics*, *10*(1), 379–393. https://doi.org/10.1029/RG010i001p00379

Lemaitre, G., & Vallarta, M. S. (1933). On Compton's latitude effect of cosmic radiation. *Physics Review*, *43*(2), 87–91. https://doi.org/10.1103/PhysRev.43.87

Leske, R. A., Mewaldt, R. A., Stone, E. C., & vonRosenvinge, T. T. (2001). Observations of geomagnetic cutoff variations during solar energetic particle events and implications for the radiation environment at the space station. *Journal of Geophysical Research*, *106*(A12), 30,011–30,022. https://doi.org/10.1029/2000JA000212

Mazur, J., Friesen, L., Lin, A., Mabry, D., Katz, N., Dotan, Y., et al. (2013). The Relativistic Proton Spectrometer (RPS) for the Radiation Belt Storm Probes mission. *Space Science Reviews*, *179*(1-4), 221–261. https://doi.org/10.1007/s11214-012-9926-9

Morfill, G. E., & Quenby, J. J. (1971). The entry of solar protons over the polar caps. *Planetary and Space Science*, *19*(11), 1541–1577. https://doi.org/10.1016/0032-0633(71)90013-4

O'Brien, T. P., Mazur, J. E., & Looper, M. D. (2018). Solar energetic proton access to the magnetosphere during the 10–14 September 2017particle event. *Space Weather*, *16*, 2022–2037. https://doi.org/10.1029/2018SW001960

Ogliore, R. C., Mewaldt, R. A., Leske, R. A., Stone, E. C., & von Rosenvinge, T. T. (2001). A direct measurement of the geomagnetic cutoff for cosmic rays at space station latitudes. *In Proceedings of the 27th International Cosmic Ray Conference*, 10, Hamb., Germany (pp. 4112).

Onsager, T. G., Grubb, R., Kunches, J., Matheson, L., Speich, D., Zwickl, R., & Sauer, H. (1996). Operational uses of the GOES energetic particle detectors, in GOES-8 and beyond. In E. R. Washwell (Ed.) *Proc. SPIE* (Vol. 2812, pp. 281-290). Bellingham, WA. https://doi.org/10.1117/12.254075

Paulikas, G. A. (1974). Tracing of high-latitude magnetic field lines by solar particles. *Reviews of Geophysics*, *12*(1), 117–188. https://doi.org/10.1029/RG012i001p00117

Paulikas, G. A., & Blake, J. B. (1969). Penetration of solar protons to synchronous altitude. *Journal of Geophysical Research*, *74*(9), 2161–2168. https://doi.org/10.1029/JA074i009p02161

Pereyaslova, N. K. (1982). Solar protons in the Earth's magnetosphere. In Energetic particles in the Earth's magnetosphere, Apatity, 3–25.

Qin, M., Hudson, M. K., Kress, B. T., Selesnick, R., Engel, M., Li, Z., & Shen, X. (2019). Investigation of solar proton access into the inner magnetosphere on 11 September 2017. *Journal of Geophysical Research: Space Physics*, *124*, 3402–3409. https://doi.org/10.1029/2018JA026380

Reames, D. V. (1999). Particle acceleration at the Sun and in the heliosphere. *Space Science Reviews*, *90*(3–4), 413–491. https://doi.org/10.1023/A:1005105831781

Richard, R. L., El-Alaoui, M., Ashour-Abdalla, M., & Walker, R. J. (2002). Interplanetary magnetic field control of the entry of solar energetic particles into the magnetosphere. *Journal of Geophysical Research*, *107*(A8), 1184. https://doi.org/10.1029/2001JA000099

Rodriguez, J. V. (2012). Undulations in MeV solar energetic particle fluxes in Earth's magnetosphere associated with substorm magnetic field reconfigurations. *Journal of Geophysical Research*, *117*, A06229. https://doi.org/10.1029/2012JA017618

Rodriguez, J. V., Krosschell, J. C., & Green, J. C. (2014). Intercalibration of GOES 8-15 solar proton detectors. *Space Weather*, *12*(1), 92–109. https://doi.org/10.1002/2013SW000996

Rodriguez, J. V., Onsager, T. G., & Mazur, J. E. (2010). The east-west effect in solar proton flux measurements in geostationary orbit: A new GOES capability. *Geophysical Research Letters*, *37*, L07109. https://doi.org/10.1029/2010GL042531

Scholer, M. (1975). Transport of energetic solar particles on closed magnetospheric field lines. *Space Science Reviews*, *17*(1), 3–44. https://doi.org/10.1007/BF00718836

Selesnick, R. S., Baker, D. N., Jaynes, A. N., Li, X., Kanekal, S. G., Hudson, M. K., & Kress, B. T. (2014). Observations of the inner radiation belt: CRAND and trapped solar protons. *Journal of Geophysical Research: Space Physics*, *119*, 6541–6552. https://doi.org/10.1002/2014JA020188

Selesnick, R. S., Baker, D. N., Kanekal, S. G., Hoxie, V. C., & Li, X. (2018). Modeling the proton radiation belt with Van Allen probes relativistic electron-proton telescope data. *Journal of Geophysical Research: Space Physics*, *123*, 685–697. https://doi.org/10.1002/2017JA024661

Sellers, F. B., & Hanser, F. A. (1996). Design and calibration of the GOES 8 particle sensors: The EPS and HEPAD, in GOES-8 and beyond. In E. R. Washwell (Ed.), *Proc. SPEI* (Vol. 2812, pp. 353-364). Bellingham, WA.

Shea, M. A., & Smart, D. F. (2012). *Space Science Reviews*, *171*(1-4), 161–188. https://doi.org/10.1007/s11214-012-9923-z

Smart, D. F., & Shea, M. A. (2005). A review of geomagnetic cutoff rigidities for Earth-orbiting spacecraft. *Advances in Space Research*, *36*(10), 2012–2020. https://doi.org/10.1015/j.asr.2004.09.015

Space weather events of 4–10 September 2017 (2017), Space Weather, **16**

Spence, H. E., Reeves, G. D., Baker, D. N., Blake, J. B., Bolton, M., Bourdarie, S., et al. (2013). Science goals and overview of the radiation belt storm probes (RBSP) energetic particle, composition, and thermal plasma (ECT) Suite on NASA's Van Allen Probes mission. *Space Science Reviews*, *179*(1-4), 311–336. https://doi.org/10.1007/s11214-013-0007-5

Störmer, C. (1955). *The polar aurora*. Press, London, England: Oxford University.

Swann, W. F. (1933). Application of Liouville's theorem to electron orbits in the Earth's magnetic field. *Physics Review*, *44*(3), 224–227. https://doi.org/10.1103/PhysRev.44.224